NAIC-ID(RS)T-0557-96

NATIONAL AIR INTELLIGENCE CENTER

SELECTED ARTICLES

Approved for public release: distribution unlimited

HUMAN TRANSLATION

NAIC-ID(RS)T-0557-96 16 January 1997

MICROFICHE NR:

SELECTED ARTICLES

English pages: 23

Source: Unknown

Country of origin: China
Translated by: Leo Kanner Associates
F33657-88-D-2188
Requester: NAIC/TATC/Bruce Armstrong

PREPARED BY:

TRANSLATION SERVICES
NATIONAL AIR INTELLIGENCE CENTER
WPAFB, OHIO

TABLE OF CONTENTS

GRAPHICS DISCLAIMER

All figures, graphics, tables, equations, etc. merged into this translation were extracted from the best quality copy available.

EXPERIMENTAL STUDY OF DEFORMATION OF COPPER MIRRORS IN A HIGH-POWER LASER SYSTEM

Xia Jinan, Zhang Yaoning,
Cheng Zuhai, and Qiu Junlin

National Laboratory of Laser Technology
Huazhong University of Science
and Technology
Wuhan 430074

Abstract: The distortion mechanism of high-power laser mirrors is discussed. The deformation of a water-cooled cavity copper mirror and an annular channel copper mirror was tested with a Twyman-Green interferometer and an imaging system. In addition, a new kind of copper mirror is proposed. Compared with the other mirrors, the new mirror has not only a small thermal deformation caused by an incident laser but also a very small pressure deformation exerted by the cooling fluid.

KEY WORDS: copper mirror, mirror distortion.

1. Introduction

When irradiated with a high-power laser, a mirror can absorb some of the energy and generate partial thermal stresses and strains, causing a change in the beam reflection field and beam spot pattern. The higher the laser power, the more heat will be absorbed by the mirror per unit time, and the larger deformation

it will cause. This phenomenon, in a laser device, will lead to an increase in the resonant cavity laser mode disturbance and losses and will affect the laser output power and beam properties[1,2]. Under severe conditions, the laser output power and output beam quality will greatly decrease. Therefore, it is necessary to take effective measures to suppress the thermal deformations of the mirror, i.e., to minimize or completely eliminate them.

Normally, the method used to control thermal deformations resulting from high-power laser irradiation is cooling the mirror[3,4]. However, during cooling, the mirror may undergo additional deformation under the pressure of the cooling fluid. To avoid this problem, a proper mirror cooling arrangement or a proper cooling solution should be specially designed.

Adopting this procedure, first the authors used a Twyman-Green interferometer and an imaging system to test, under cooling conditions, the surface shape of a laser-affected mirror, and then studied, respectively, the pressure deformations due to the cooling medium and the laser-induced thermal deformations of the cavity copper mirror and the annular-channel copper mirror. Also, we designed a copper mirror with a multilayer cooling structure and compared and analyzed the three structure copper mirrors.

2. Experimental Study of Copper Mirror Deformation

The experiment system is shown in Fig. 1, in which laser$_1$ is a high-power laser source; laser $_2$ is a Twyman-Green interferometer laser source, namely a helium/neon tube; M_t is the objective lens to be measured; M_r is the reference mirror; M is an ordinary reflection mirror; E is a beam-expander; L is a collimating lens; B_s is a beam splitter, while the imaging system

is composed of a CCD video camera, a monitor, a computer, and a printer.

Fig. 2 (a) and (b), respectively, are schematic diagrams of the simple-cavity copper mirror and the annular-channel copper mirror. In general, these two types of copper mirror are applicable in some laser systems, but they display an overly high deformation value in other systems, where vigorous requirements are imposed on deformation.

Hence, we designed a new copper mirror with a multilayer structure as indicated in 2(c). Experiments showed that this mirror generates very slight deformations. The reason for this is as follows: during mirror deformations, on the one hand, the laser thermal action can cause a nonuniform temperature distribution of the mirror, resulting in thermal stresses and thermal expansion; on the other hand, under the pressure of the cooling fluid, the mirror is subjected to a certain amount of load so as to undergo strain. However, the new copper mirror showed more satisfactory cooling effects; it was subjected to small partial thermal stresses, high structural strength, and low pressure deformation. As a result, its overall deformation was relatively small.

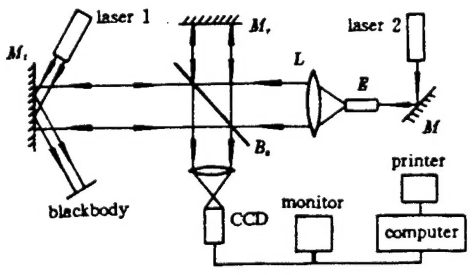

Fig. 1. Schematic of Twyman-Green interferometer and imaging system

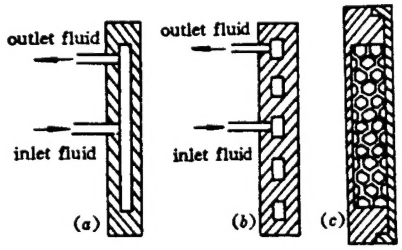

Fig. 2. (a) cavity-structure mirror (b) annular-channel mirror (c) new structure type mirror

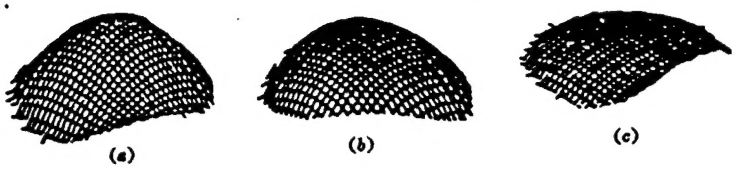

Fig. 3. (a) deformed surface of a cavity copper mirror (b) deformed surface of an annular channel mirror (c) deformed surface of new copper mirror

2.1. Mirror Surface Deformation Regularities When Mirror Is Subjected to Laser Irradiation

The surface shape of the mirrors deformed under laser irradiation is shown in Fig. 3. Fig. 3(a), (b) and (c), respectively, indicate the surface shape of the cavity mirror, the annular-channel mirror, and the multilayer structure mirror under the same laser power, the same flow of cooling fluid, and the same pressure. The original surface of the three copper mirrors was flat, their diameter was 68mm, laser irradiance was 350W, spot diameter was 25mm; the laser was nearly a basic mode, and the water cooling pressure was 0.2MPa.

It can be seen from the figure that for all the mirrors each surface shows a tendency of convexity, among which, the cavity mirror is the most convex, followed by the annular channel mirror, while the new copper mirror is convex the least. This suggests that the cavity copper mirror was deformed most severely, followed by the annular channel mirror, while the new copper mirror was deformed the least.

This is also reflected in the relative value and location of the curves shown in Fig. 4. Fig. 4 illustrates the maximum

deformation of the mirrors versus incident laser power when the cooling fluid pressure is 0.2MPa, where the curve value of the cavity copper mirror is much larger than that of the other two mirrors, while the curve value of the new copper mirror appears extremely small, which reflects the foregoing statement. The ordinate in the figure is the maximum deformation of the mirror surface, while the abscissa is incident laser power. In fact, with cooling fluid, the mirror deformation is primarily caused by two factors: one factor is the thermal process of the laser, while the other factor is the pressure of cooling fluid.

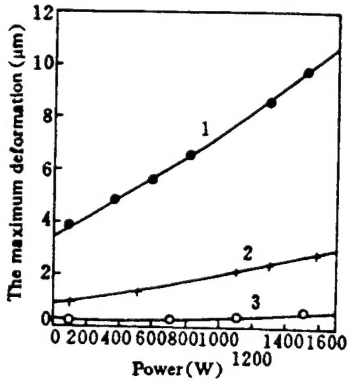

Fig. 4. Maximum deformation versus incident laser power when cooling fluid pressure is 0.2MPa
KEY: 1 - cavity copper mirror 2 - annular-channel mirror 3 - new copper mirror

2.2. Effect of Cooling Fluid Pressure on Mirror Deformation

Fig. 5 shows the maximum surface deformation of the different structural types of mirrors versus cooling medium pressure without laser irradiation. Here, the cooling medium is water, and the surface diameter of the mirrors is ϕ68mm. The figure indicates that the maximum surface deformation of the mirrors increases nearly linearly with increase in cooling medium pressure, in which case the cavity mirror is deformed the most, much more than the other two mirrors. Thus, it is not wise to adopt the cavity cooling structure in designing a mirror, though such kind of mirror is simple to process. The deformation of the

annular-channel mirror can be remarkably improved as confirmed by the relative location of curve 2 in Fig. 5, but even so, this mirror still cannot meet the requirements in highly demanding resonant cavities.

The deformations of the new mirror, namely the multilayer structure mirror, as shown in Fig. 5, are very small. Therefore, this kind of mirror can effectively suppress the mirror deformations caused by cooling medium pressure. As a matter of fact, the effect of cooling fluid pressure on mirror deformation varies with the change in the structural strength of the mirror, i.e., the higher the mirror structural strength, the smaller the deformation resulting from cooling fluid pressure, or visa versa. In this case, Fig. 5 suggests that the structural strength of the new mirror proves to be higher than that of the other two mirrors.

Fig. 5 also suggests when the fluid-cooled mirror is adopted to remove or control the thermal deformation caused by a high-power laser system, additional deformation, i.e., pressure deformations may occur that are by no means caused by the laser itself. Therefore, selecting a cooled copper mirror structure for a laser system must be based on the actual conditions, and it is recommended to select a mirror with higher structural strength.

2.3. Thermal Deformations Caused by Laser Action

Fig. 6 shows the thermal deformations for different structure copper mirrors versus incident laser power under laser irradiation when the cooling fluid pressure was 0.2MPa, where the curves represent the values excluding the pressure deformations. In the figure, the spot diameter of the incident beam is approximately 25mm, nearly a basic mode; the surface reflectivity of the cavity mirror is 0.975; the surface reflectivity of the

annular channel copper mirror is 0.98; the surface reflection of the new mirror is 0.982; the structure and dimension of these mirrors are the same as mentioned above.

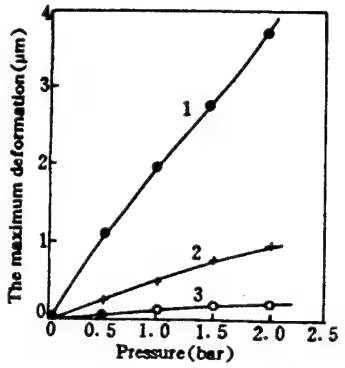

Fig. 5. Maximum deformation versus cooling fluid structure
KEY: 1 - cavity copper mirror
2 - annular copper mirror
3 - new copper mirror

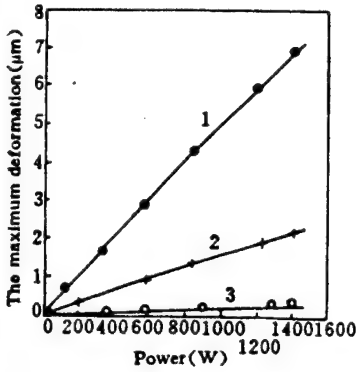

Fig. 6. Maximum deformation versus laser power
KEY: 1 - cavity copper mirror 2 - annular copper mirror 3 - new mirror

It can also be seen from Fig. 6 that under particular cooling conditions, the laser-induced thermal deformation of the mirrors increases with increase in incident laser power: the higher the power, the larger the deformation. From the relative location of the curves as indicated in Fig. 6, the cavity mirror has the largest surface thermal deformation, the annular-channel mirror is next, and the new copper mirror has the smallest surface thermal deformation, which is determined by different cooling effects of different copper mirrors. The cavity copper mirror has the poorest cooling effect, the annular channel copper mirror is the next, while the new copper mirror has the best cooling effect.

It can also be seen from the relative location of the curves that compared with the cavity copper mirror, the cooling effect of the annular-channel mirror can be greatly improved. However, this mirror is still not as good as the new copper mirror. This also indicates that the cooling effect of the annular channel

copper mirror is not as good as that of the new copper mirror.

3. Conclusions

In a high-power laser system, a mirror can absorb some of the surface energy and be subjected to thermal stress and thermal deformation. When the deformation exceeds a certain value, it may affect the performance of the system. For instance, it can cause the laser output power drop or the beam equality decrease. Therefore, effective measures must be adopted in order to control the mirror deformation, namely, to minimize it or completely eliminate it.

In normal circumstances, this can be realized through the mirror cooling technique, but in this case, the mirror may be subjected to additional deformation due to cooling fluid pressure. Thus, the structure of the mirror should be specially selected and well designed so that the mirror has high structural strength and good cooling effects and becomes optimal. Otherwise, the mirror will be subjected to greater deformation.

The experimental study of the cavity, annular channel and new multilayer structure copper mirrors as described in this paper proved that the cavity mirror has the poorest cooling effect, low structural strength, and accordingly, larger thermal deformation and pressure deformation; therefore, it is not to be recommended.

As for the annular channel copper mirror, its laser-induced thermal deformation and the cooling fluid pressure deformation can be greatly improved, and effectively suppressed as long as the laser power is not so high, can be effectively suppressed. However, its deformation is still slightly higher with reference to a higher power laser system or in the case when vigorous requirements are set for deformation.

While the new copper mirror can provide satisfactory results because this mirror not only shows a high structural strength, but also good cooling effects. Therefore, its thermal deformation caused by the laser process and the pressure deformation caused by the cooling fluid are both relatively small, which can serve as an effective solution for suppressing the mirror surface deformation in a laser system.

REFERENCES

1. Zhou Binkun, Principles of Lasers, Chengdu, National Defense Industry Publishing House, 1987, pp. 129-133.

2. Lu Baida, Laser Optics, Chengdu, Sichuan University Publishing House, 2nd ed., 1991, pp. 335-358.

3 Yuen W. W. , Fleishman R. V.. A Parameteric Study of Mesh Enhanced Forced Convection Heat Transfer for the Cooling of High Power Density Mirror. *SPIE*. 1989. **1047** : 43～55

4 Anthony F. M. , Hopkins A. K.. Actively Cooled Silicon Mirrors. *SPIE*. 1981. **2978** : 196～203

This paper was received for editing on August 1, 1995, and the edited paper was received on October 30, 1995.

SPACE SPECTRUM AND FILTERING OF APERTURED BESSEL BEAM

Jiang Zhiping, Liu Zejing,
Lu Qisheng, and Zhao Yijun

Department of Applied Physics
National University of Defense Technology
Changsha 410073

Abstract: The space spectra of the apertured Bessel beam are calculated. The propagation of the apertured Bessel beam is discussed in relation to the space spectrum. The criteria of the nearly diffraction-free beam are as follows: the space spectrum has a non-zero major maximum and the spectral widths are narrow. The propagation feature can be improved through space filtering.

KEY WORDS: Bessel beam, aperture, space spectrum, filtering.

1. Introduction

Researchers are interested in a "diffraction-free" beam-Bessel beam primarily for two reasons: one reason is that, theoretically, the "diffraction-free" or "super-diffracting" beam has long been a research goal, while the Bessel beam demonstrated a possibility of achieving this goal. The other reason lies in its applications: a very fine central major maximum can remain basically unchanged during long-range propagation; therefore, the beam is expected to be applied in various fields, such as super-precision collimation, large- and deep-caliber laser boring, communications, and energy transmission.

In this situation, since 1987 when Durnin et al. first published reports on experiments with Bessel beams[1-3], great interest has been stirred in this topic in the optical research community, and very much research was done on these beams, their propagation and applications. Even today, numerous papers on this field have been published[4-8].

Diffraction is an essential feature of light that any other wave motion phenomenon cannot surpass. Literally, a "diffraction-free" or "super-diffracting" beam does not exist, including even the Bessel beam. The Bessel beam serves as a solution to wave-motion equations. When we say a beam is diffraction-free, we mean it does not change with propagation distance. It appears as if it is diffraction-free, but in fact, this feature is just the result of diffraction; only in this case, the diffraction is extremely subtle.

Another feature of the Bessel beam is that its total energy is infinite, indicating the physically ideal Bessel beam does not exist. All physically significant Bessel beams are ideal Bessel beams restricted by a particular aperture[3]. The aperture can be either a hard-edge aperture (small holes) or a soft-edge aperture (such as Gaussian aperture, i.e., Gaussian-Bessel aperture[6]). An apertured Bessel beam also has a "diffraction-free" character: its distribution remains basically unchanged at a particular propagation distance.

The authors studied the propagation of apertured Bessel beams with respect to the space spectrum, aiming at a physical picture for understanding the propagation of the apertured Bessel beam, and to propose, on this basis, a space filtering method to improve its propagation feature.

2 Space Spectrum of Apertured Bessel Beam

A Bessel beam is column-symmetric. Let f(r) be the aperture

function, and $J_0(\alpha r)$ be the Bessel function, then the space spectrum can be derived through zero-order Henkel transformation[9]:

$$G(\rho) = 2\pi \int_0^{\infty} f(r) J_0(\alpha r) J_0(2\pi r \rho) r dr \tag{1}$$

When f(r)=1 (i.e., aperture-free), Eq. (1) can offer the space spectrum of an ideal Bessel beam as follows:

$$G(\rho) = \frac{1}{\alpha}\delta\left(\frac{\alpha}{2\pi} - \rho\right) \tag{2}$$

Eq. (2) implies that the space spectrum of an ideal Bessel beam is a cone face. This is Gori's explanation[6]: a Bessel beam can be regarded as a number of superimposed plane waves whose wave vectors are all distributed on the surface of a cone with propagation direction z as the center as shown in Fig. 1(a), while Fig. 1(b) is the space spectrum. When a beam is apertured, its spectrum becomes much more complex. Given $f(\rho)$ as the Hankel transform of f(r), the space spectrum of the apertured beam can be derived through convolution[9] as follows:

$$G(\rho) = \int_0^{\infty} \int_0^{2\pi} F(\zeta) \frac{1}{\alpha}\delta\left(\frac{\alpha}{2\pi} - R\right) \zeta d\zeta d\theta \tag{3}$$

where

$$R = \sqrt{\rho^2 + \zeta^2 - 2\rho\zeta\cos\theta}$$

In our formalism, Eq. (3) is not simpler than Eq. (1), yet from it some useful results can be obtained. In Eq. (3), the contributions of ζ and Θ should satisfy $R=\alpha/2\Pi$, i.e., the following is necessary:

$$\zeta = \rho\cos\theta \pm \sqrt{(\alpha/2\pi)^2 - \rho^2\sin^2\theta} \tag{4}$$

so

$$G(0) = 2\pi F(\alpha/2\pi) \tag{5}$$

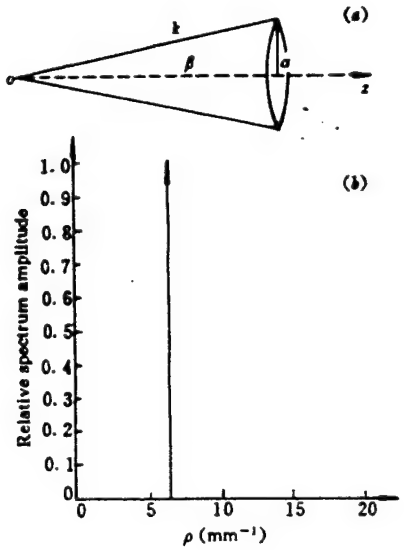

Fig. 1
(a) the wave vectors of the ideal Bessel beam
(b) the space spectrum (α=40 mm^{-1})

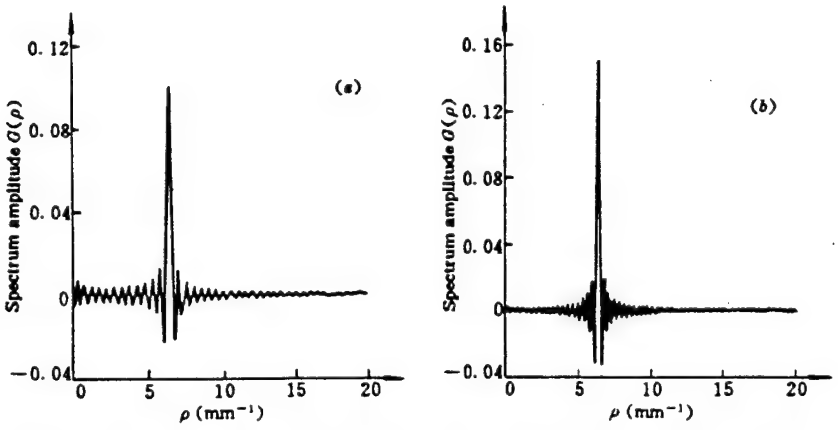

Fig. 2. Space spectra of circular truncated Bessel beams with α=40mm^{-1} and radii (a) 2mm; (b) 3mm

The hard-edge aperture and Gaussian aperture are two most commonly used apertures, for which we calculated their respective space spectra with α=40cm^{-1}. Fig. 2 shows the spectrum with a hard-edge aperture; the aperture radii corresponding to Fig. 2 (a) and (b), respectively, are 2mm and 3mm. Fig. 3 is the space spectrum with a Gaussian aperture, and the aperture radii corresponding to Fig. 3 (a) and (b) are, respectively, 2mm and 3mm. The spectra feature a peak value of higher intensity; its location rho_{max} is

derived from $\alpha/2\Pi$; its width is inversely proportional to the diameter of aperture, while its altitude is directly proportional to the aperture diameter. The width of the central major maximum of the Bessel beam is $1/\alpha$; therefore, the smaller this width, the larger ρ_{max} can be.

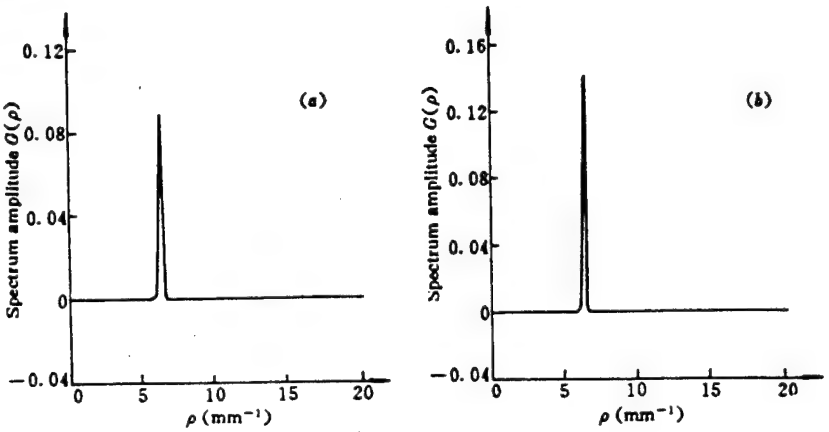

Fig. 3. The space spectra of the Gauss-Bessel beams with α=40mm^{-1} and Gaussian radii (a) 2mm; (b) 3mm

By calculating the propagation of the Bessel beam after axicon transformation, it was found that a negative axicon can increase the axial light intensity but decrease the z_{max}, the distance at which the beam basically remains unchanged; in contrast, a positive axicon will decrease the axial light intensity with increase in z_{max}[10]. Hence, an axicon not only can be used to generate Bessel beams, but also is a powerful tool in transforming Bessel beams. The transmittance of the axicon can be derived from the following formula:

$$T(r) = \exp(\pm i\gamma r) \tag{6}$$

The symbol plus corresponds to the negative axicon, while the symbol minus corresponds to the positive axicon. At this instant, the spectrum should be:

$$G(\rho) = 2\pi \int_0^{\infty} f(r) \exp(\pm i\gamma r)\, J_0(\alpha r)\, J_0(2\pi\rho r) r\, dr \tag{7}$$

Eq. (7) suggests that following axicon transformation, the spectrum of the Bessel beam will be a plural number. At the spectrum face, the negative and positive axicons share the same intensity

distribution but will differ in phase distribution by a minus, which is extremely important in understanding the effects of the negative and positive axicons. Fig. 4 is Fig. 2(a) as follows: the space spectrum of the Bessel beam with a hard-edge aperture after passing through a negative axicon, $\gamma=10mm^{-1}$. Fig. 4(a) is $|G(\rho)|$, while Fig. 4(b) is the phase distribution. With an axicon, the spectrum changes from one main peak to two main peaks; the locations of the two peaks are, respectively, the difference and sum of the axicon frequency and the original Bessel beam frequency, because the two frequencies are in multiplication relations.

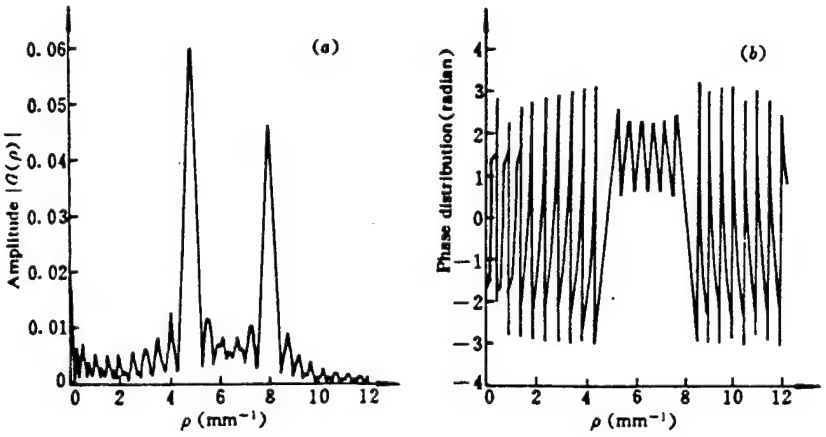

Fig. 4. Space spectra of the circular truncated Bessel beams passing through a negative axicon.
(a) absolute amplitude distribution
(b) phase distribution, $\alpha=40mm^{-1}$, circular radius is 2mm, $\gamma=10mm^{-1}$

Noting that the focal plane of lens can produce beam spectra, it is assumed that Fig.1(b), Fig. 2 and Fig. 3 actually show the amplitude distribution at the lens focal plane. The result given in Fig. 1(b) is interesting, which indicates that an ideal Bessel beam cannot be focused. Indeed, an ideal bessel beam cannot be focused in reality, because this requires that the radius of lens be infinite. However, it can be seen from Figs. 2 and 3 that the more ideal the Bessel beam is, the smaller the axial light intensity. Eq. (5) provides the light amplitude at the focal point of the apertured Bessel beam; generally speaking, the larger the

aperture, the larger the α, and the smaller the light amplitude at the focal point. Reference [8] discusses the focusing of the Bessel beam, Eq. (5) serving as its supplement.

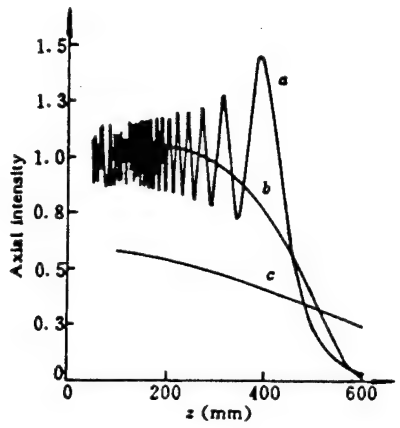

Fig. 5. Axial intensity distributions (a) circular truncated Bessel beam, $\alpha=40mm^{-1}$, radius is 2mm (b) after low-pass filtering of (a), cut-off frequency $7.0mm^{-1}$ (c) after bandpass filtering of (a), passband is $6.26-6.48mm^{-1}$

3. Discussion of Propagation of Apertured Bessel Beam in Terms of Space Spectrum

The space spectrum of an ideal Bessel beam is a function of δ, and the role of an aperture is to excite many Bessel beams with other space spectra. Thus, the propagation of an apertured Bessel beam can be regarded as the result of interference from many Bessel beams (weighted according to spectra in Figs. 2 and 3). For instance, the axial amplitude can be derived from the following formula:

$$E(z) = \int_0^\infty G(\rho) \exp(i\beta z)\rho \, d\rho \tag{8}$$

where $\beta = \sqrt{k^2 - (2\pi\rho)^2} \approx k - (2\pi\rho)^2/2k$, k is the number of waves. Eq. (8) can be written as follows:

$$E(z) = \exp(ikz) \int_0^\infty G(\rho) \exp\left[-i\frac{(2\pi\rho)^2}{2k}z\right]\rho \, d\rho \tag{9}$$

Eq. (9) very much resembles the interference from a fraction of the coherent light of nonrigorous monochromatic light[11]. z_{max}, the distance at which the axial amplitude basically remains unchanged, depends on $\Delta\rho_{eff}$, the effective width of G(p): the smaller the $\Delta\rho_{eff}$, the larger the z_{max}, and visa versa. The term effective width is used because $G(\rho)$ is fairly complex, and its width cannot be given as easily as the Gaussian function.

For an ideal Bessel beam, its spectrum is a function of δ [Eq. (3)], and its axial amplitude given in Eq. (11) is a constant. When the beam is apertured, $G(\rho)$ is no longer a function of δ but a function of distribution; E(z) is a function of distance. It is easy to understand that if $G(\rho)$ changes, E(z) will be also change. For a hard-edge apertured (small hole) truncated Bessel beam, E(z) takes the form of a curve as shown in Fig. 5(a) (α=40mm^{-1}; the aperture is 2mm). Although E(z) remains basically unchanged within the distance z_{max}, E(z) is fluctuating; the closer to z_{max}, the more vibrating E(z) can be. In actual applications, E(z) is expected to be unchanged (such as in laser boring), or z_{max} is expected to be larger (such as in laser collimation), which can be realized through space spectrum filtering, such as through the solution of the following formula:

$$\int_0^{\infty} G(\rho)\exp\left(-i\frac{(2\pi\rho)^2}{2k}z\right)\rho\,d\rho=\begin{cases}1, & z\le z_{max}\\ 0, & z>z_{max}\end{cases} \qquad (10)$$

In fact, Eq. (10) is an ideal formula and is not likely to be solved in a strict sense, but can be solved in the sense of minimum variance.

The exponential factor in Eq. (9) indicates that when z is fairly small, the vibration of axial intensity originates from a large space spectrum component, and can be reduced by filtering the high frequency component as seen in Fig. 5(b). Fig. 5(b) shows the result of filtering the above-7.0mm^{-1} light from the space spectrum, where the vibration frequency of axial intensity has been greatly

reduced. By narrowing the space spectrum distribution $G(\rho)$, z_{max} can be enlarged as shown in Fig. 5(c), which can be achieved, of course, at the expense of a decrease in light intensity. In addition, Eq. (9) can be written as:

$$E(z) = \int_0^{\infty} |G(\rho)| \exp\left[i\varphi(\rho) - i\frac{(2\pi\rho)^2}{2k}z\right]\rho\, d\rho \qquad (11)$$

In Eq. (11), the phase factor exp(ikz) that does not affect the light intensity is omitted, where $\phi(\rho)$ is the phase factor of $G(\rho)$. The second phase factor in Eq. (11), $[(2\Pi\rho)^2/2k]z$, suggests that the light with a high space spectrum underwent a greater phase change than the light with a low space spectrum; the phase factor $\phi(\rho)$ put a phase difference between the two lights in advance. Noting the phase distribution of the space spectrum of the axicon, it is easy to comprehend the transformation of the Bessel beam by the axicon. For instance, the spectral energy of a negative axicon in Fig. 4 is concentrated at two peaks: the low-frequency peak $(\alpha-\gamma)/2\Pi$ (approximately $4.77mm^{-1}$), and the high-frequency peak $(\alpha+\gamma)/2\Pi$ (approximately $7.96mm^{-1}$) [Fig. 4(a)]. From the view of phase distribution, at $4.77mm^{-1}$, the high frequency is lagging and the low frequency is advancing, while at $7.96mm^{-1}$, the situation is just the opposite. Thus, at $4.77mm^{-1}$, the spectral phase $\phi(\rho)$ forces the phase factor in Eq. (11) not to exceed Π over longer distances, and thus increase z_{max}. Literally speaking, the factor that runs slower runs first, and the factor that runs faster runs later so that they can keep basically the same phase over a longer distance. While the spectral peak at $7.96mm^{-1}$ shows an entirely different picture, i.e., the factor that runs faster runs first, and the factor that runs slower runs later; as a result, the phase is compensated and interfered, and the spectral peak no longer is in effect.

Since the space spectrum of the effective spectral peak is smaller than that without the negative axicon, the width of the central major maximum of the beam will increase (approximately $1/\alpha$) with the negative axicon compared with its original width. The

case is reverse with the positive axicon.

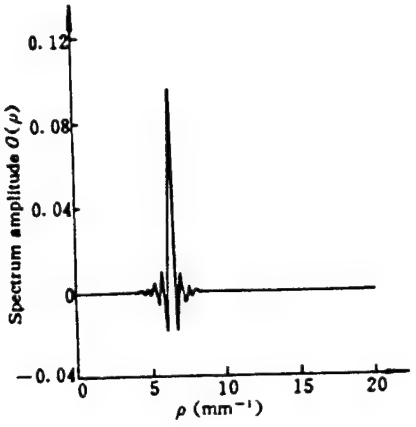

Fig. 6. Space spectrum of the supergaussian-bessel beam [Eq. (15)], α=40mm^{-1}, w=2mm

Eq. (9) indicates that if $G(\rho)$ has a peak value at $\rho=\rho_{max}$, and the effective width is $\Delta\rho_{eff}$, then when ρ_{max} is much larger than $\Delta\rho_{eff}$, z_{max}, the distance, at which E(z) basically remains unchanged, can roughly be given in the following formula:

$$\frac{4\pi^2\rho_{max}\Delta\rho_{eff}}{k} z_{max} \approx \pi \qquad (12)$$

For the circular-hole apertured bessel beam, $\rho_{max}=\alpha/2\Pi$, $\Delta\rho_{eff}$ can be regarded as the frequency corresponding to the first dark ring of the circular hole, i.e., the selection of is reasonable, where D is aperture. Therefore,

$$z_{max} \approx \pi D/\alpha\lambda \qquad (13)$$

This is the result presented in reference [2]. Of course, the foregoing selection of $\Delta\rho_{eff}$ is somewhat random but reasonable, which suggests that it is rational to discuss the propagation of an apertured Bessel beam from the angle of space spectrum.

Also, we can reach another conclusion: for gently changing beams including Gaussian beam, $\rho_{max} \approx 0$. In this case, Eq. (12) is not

applicable; instead, we must use

$$\frac{(2\pi\Delta\rho_{eff})^2}{2k} z_{max} \approx \pi \tag{14}$$

By comparing Eqs. (14) and (12), it is easy to find that the distance, at which the axial intensity basically remains unchanged, is much greater in the apertured Gaussian beam than in the apertured Bessel beam, because the change of axial intensity basically reflects the diffusion of the beam. Based on this, we can conclude that the propagation property of the Bessel beam is poorer than that of the Gaussian beam.

This conclusion may appear surprising. However, just as Sprangle and Hafizi explained [12], Durnin held that the Bessel beam has a greater "non-diffusion" distance only because he evaluated the Gaussian beam radius to be equal to the radius of the central major maximum of the Bessel beam. In fact, the radius of the Gaussian beam should be evaluated as the entire dimension of the Bessel beam so that the Gaussian beam should have a greater "non-diffusion" distance.

If this is so, how shall we understand the "diffraction-free" property of the apertured Bessel beam? Our point is: when we speak of the "diffraction-free" property of the apertured Bessel beam, we mean that its finer central major maximum has a greater "non-diffusion" distance (e.g., compared with the Gaussian beam of the same dimension). To possess such a "non-diffusion" property, the space spectrum of the beam should meet the following two conditions: 1. The light that occupies the majority of energy should have higher space spectrum so that a sufficiently fine central major maximum can exist; 2. The space spectrum should be fairly concentrated so as to ensure a greater "diffraction-free" distance. Eq. (12) shows that the "diffraction-free" distance z_{max} is inversely proportional to z_{max} and ρ_{max}.

4. Space Filtering

Here, space filtering has two implications: first, it is ordinary space filtering, such as the commonly used 4f optics system, which can, through filtering of the incident apertured Bessel beam, eliminate (weaken) the vibration of light intensities, or enlarge z_{max}. The other implication is that the generation of the Bessel beam. Since we already discussed the ordinary space filtering earlier in this paper, we will focus on the generation of the Bessel beam here.

Given a beam, its space spectrum can be derived through a Fourier transform; similarly, given a spectrum, its corresponding beam can be derived through a Fourier transform. The spectrum of an ideal Bessel beam has a width equal to the bright ring of zero; therefore, an approximate beam can be derived through fourier transformation of the fine ring. This technique was applied by Durnin et al., in generating the Bessel beam in their first demonstrative experiment[3]. In that case, with an appropriate space filter, the required spectrum distribution can be obtained from the incident plane wave. This technique can be used to generate the required truncated Bessel beam. For instance, calculations show that the following Super-Gaussian-Bessel (SGB) beam is a "real" diffraction-free beam over a particular propagation distance; the change of its intensity distribution is much smaller than that of the hard-hole truncated Bessel beam and virtually unchanged[13]:

$$U^{SGB}(r) = \exp\left[-\left(\frac{r}{w}\right)^{15}\right] J_0(\alpha r) \tag{15}$$

We can calculate the spectrum in Eq. (15). For instance, in Fig. 6, let α=40mm^{-1}, and w=2mm, the spectrum is solid. With this, the Super-Gaussian-Bessel beam can be realized by making a corresponding filter through photography or space optical modulator plus a simple lens.

5. Conclusions

The Bessel function is the solution of the Helmholtz equation, while the space spectrum of an ideal Bessel beam is a function of δ (actually, a ring face due to columnar symmetry). When a beam is apertured, its space spectrum expands to generate Bessel beams with other space spectra, and the field is coherent superimposition of these Bessel beams. In z_{max}, the vibration of axial light intensity originates from the contribution of the space spectra away from the center. By filtering the light of these space spectra, the vibration of the axial light intensity can be eliminated, which is favorable to some applications (such as laser boring).

In addition, z_{max}, the distance, at which the central major maximum of the apertured Bessel beam remains basically unchanged, primarily depends on the width of the Fraunhofer diffraction of the aperture major maximum; z_{max} can be increased through decreasing the foregoing width. It is easy to comprehend the effect of axicon on the apertured bessel beam from the angle of space spectrum. The space spectrum filtering can be either amplitude filtering or phase filtering (in the case of axicon). Generating the required apertured Bessel beams, including the supergaussian-Bessel beam from the view of space spectrum proves to be a truly simple technique.

REFERENCES

1 J. Durnin, J. J. Miceli, J. H. Eberly. Diffraction-free beams. *J. Opt. Soc. Am.*, 1986, A3 : 128

2 J. Durnin. Exact solutions of nondiffracting beams I . The scarlar theory. *J. Opt. Soc. Am.*, 1987, A4 : 651

3 J. Durnin. Diffraction-free beams. *Phys. Rev. Lett.*, 1987, 58 : 1499

4 R. M. Herman, T. A. Wiggins. Production and uses of diffractionless beams. *J. Opt. Soc. Am.*, 1991, A8 : 932-942

5 L. C. Laycock, S. C. Webster. Bessel beams; their generation and application. *GEC J. Res.*, 1992, 10 : 36～51

6 F. Gori, G. Guattari, C. Padovani. Bessel-Guass beams. *Opt. Commun.*, 1987, 64 : 491～495

7 G. Scott. Efficient generation of nearly diffraction-free beams using an axicon. *Opt. Eng.*, 1992, 31 : 2640～2646

8. Huang Wenlong, Lu Baida, Ye Yidong et al. "Axial light intensity distribution of focused Bessel-Gaussian beams with limited width," China Laser, 1995, A22(4): 285.

9. Li Jingzheng (chief editor), Optics Handbook, Xi'an: Shaanxi Science and Technology Publishing House, 1986 (1st ed.), pp. 214-215, 223.

10 Jiang Zhiping, Lu Qisheng, Liu Zejin . Propagation of apertured Bessel beams. accepted in *Appl. Opt.*,

11. Born, Max and E. Wolf. Principles of Optics, Beijing: Science Publishing House, 1985 (2nd ed.), p. 415.

12 P. Sprangle, B. Hafizi. Comment on nondiffracting beams. *Phys. Rev. Lett.*, 1991, 66 : 837

13 Jiang Zhiping. Super-Gaussian-Bessel beam. submitted to *Opt. Commun.*,

This paper was received for editing on August 14, 1995, and the edited paper was received on December 4, 1995.